PCCP
Physical Chemistry Chemical Physics

Accepted Manuscript

This article can be cited before page numbers have been issued, to do this please use: D. Akbarian, D. E. Yilmaz, Y. Cao, P. Ganesh, I. Dabo, J. MUNRO, R. Van Ginhoven and A. C. T. van Duin, *Phys. Chem. Chem. Phys.*, 2019, DOI: 10.1039/C9CP02955A.

ROYAL SOCIETY OF CHEMISTRY

rsc.li/pccp

View Article Online
DOI: 10.1039/C9CP02955A

Understanding the influence of defects and surface chemistry on ferroelectric switching: A ReaxFF investigation of $BaTiO_3$

Dooman Akbarian[1], Dundar E. Yilmaz,[1] Ye Cao[2], P. Ganesh[2], Ismaila Dabo[3], Jason Munro[3], Renee Van Ginhoven[4] and Adri C. T. van Duin[1*]*

[1] Department of Mechanical Engineering, Pennsylvania State University, University Park, Pennsylvania 16802, USA.

[2] Center for Nanophase Materials Sciences, Oak Ridge National Laboratory, Oak Ridge, Tennessee 37831, USA.

[3] Department of Materials Science and Engineering and Materials Research Institute, The Pennsylvania State University, University Park, Pennsylvania 16802, USA.

[4] Air Force Research Laboratory (AFRL), Kirtland AFB, New Mexico 87117, USA.

[*] Corresponding Author

View Article Online
DOI: 10.1039/C9CP02955A

Abstract

Ferroelectric materials such as barium titanate ($BaTiO_3$) have a wide range of applications in nano scale electronic devices due to their outstanding properties. In this study, we developed an easily extendable atomistic ReaxFF reactive force field for $BaTiO_3$ that can capture both its field- as well as temperature-induced ferroelectric hysteresis and corresponding changes due to surface chemistry and bulk defects. Using our force field, we were able to reproduce and explain a number of experimental observations: (1) existence of a critical thickness of 4.8 *nm* below which ferroelectricity vanishes in $BaTiO_3$; (2) migration and clustering of oxygen vacancies (OVs) in $BaTiO_3$ and reduction in the polarization and the curie temperature due to the OVs; (3) domain wall interaction with surface chemistry to influence ferroelectric switching and polarization magnitude. This new computational tool opens up a wide range of possibilities for making predictions for *realistic* ferroelectric interfaces in energy-conversion, electronic and neuromorphic systems.

View Article Online
DOI: 10.1039/C9CP02955A

Introduction

Ferroelectric perovskites such as barium titanate ($BaTiO_3$) have demonstrated a great potential for applications in nonvolatile memories, transducers, micro sensors and capacitors because of their unique properties such as spontaneous polarization, piezoelectric and pyroelectric effects, as well as large dielectric constants [1-5]. Recent advances in making artificial oxide heterostructures has enabled designing electronically important functional oxide interfaces as well as ferroelectric-based memristor devices[6-7]. Previous experimental studies showed that particle size and defects/dopants can significantly affect the dielectric properties of ferroelectric materials [8-11]. Extensive experimental efforts have been put into BaTiO3/polymer composites for the purpose of improving the dielectric properties by introducing high dielectric constant fillers and sol-gel method [12-14]. In order to design and optimize these devices, it is essential to obtain detailed, atomistic-scale insight of the $BaTiO_3$ ferroelectric perovskite. Currently, there are three approaches to model the ferroelectric behavior of $BaTiO_3$: phenomenological, first-principles and force field-based methods. The phenomenological methods such as the Landau-Ginzburg-Devonshire (LGD) model describe the energy of the system as a polynomial expansion of polarization, strain, temperature, external electric field and the polarization of system based on the displacement of charges [15-16]. Phase-field model, which is based on the LGD description of the ferroelectric polarization, further considers the inhomogeneous system with domain-domain interactions and long range order elastic and electric fields[17]. Although these methods can simply describe the ferroelectric perovskites, they do not consider the atomic structure of the system. First-principles methods such as the density functional theory (DFT) are considered as the most accurate models which derive the electronic structures of ferroelectric materials based on the laws of quantum mechanics [18-21]. However, because of high computational costs these first-

View Article Online
DOI: 10.1039/C9CP02955A

principles methods can only be viable for relatively small length (~5 nm) and short time scales (~100 ps) restricting investigation of hysteresis loops, sequential phase transitions and domain wall motions that occur at longer length (~10 – 100 nm)- and time(>ns)-scales. Force field based methods can provide the computational speed required to perform molecular dynamics (MD) simulations with system length and time scales sufficiently large to describe the full chemistry of the ferroelectric perovskites. Currently, there are three force field-based models available for ferroelectric perovskites including $BaTiO_3$: shell model, effective Hamiltonian model and bond-valence model. In the shell model, the valence electrons are a massless, charged shell linked to a massive charged core. In this empirical potential, the interaction between the core and shell was considered at the oxygen atoms, by harmonic and fourth-order terms for the core-shell interactions on the Ba-O planes, and the Ti-O bonds, respectively [22-23]. The shell model has been utilized in several MD studies to investigate the effects of oxygen vacancies (OVs), strain and film thickness on the polarization of $BaTiO_3$ nano-films [24-32]. However, since a very low mass was specified to the shell, a very small MD time step (~ 0.4 *fs*) in the MD simulations using this potential is essential to obtain accurate results limiting the length and the time scales of the MD simulations. An *ab-initio* based effective Hamiltonian model was developed as a function of only a small number of degrees of freedom including a local soft-mode amplitude vector and a local strain tensor [33-34]. This method has been successfully applied to some ferroelectric materials such as $BaTiO_3$ to investigate their finite-temperature properties [35-39]. The bond-valence (BV) empirical potential for ferroelectric materials includes a bond-valence vector energy term measuring the unit cell asymmetry. This potential is based on the conservation principles of the bond valence and the bond valence vector, and it has been successfully parametrized for different ferroelectric materials including $BaTiO_3$ [40-44]. Also, Goddard et al developed a potential that

View Article Online
DOI: 10.1039/C9CP02955A

allows charge flow through polarizable charges by an extended polarizable core-shell model [45]. These models can be utilized successfully within a single ferroelectric formulation, however, they cannot straightforwardly be extended to investigate the interactions of ferroelectric materials in multi-material interfaces, and cannot handle chemical reactions. One of the widely used reactive force fields is the ReaxFF reactive force field, which combines a bond order/bond distance relationship with a polarizable charge description[46-47]. In the ReaxFF the connectivity of atoms is determined by bond orders based on the interatomic distances that are updated every time step, which allows for bonds breaking and formation during the simulation. Moreover, in ReaxFF the polarization effects are calculated using a geometry-dependent charge calculation procedure based on the electronegativity equalization method (EEM) [48] which plays a key role in the modeling of $BaTiO_3$. The nonbonded interactions such as van der Waals and Coulomb interactions are determined between every pair of atoms, irrespective of connectivity, and any excessive close-range nonbonded interactions are excluded by defining a shielding term[46-47]. ReaxFF has been successfully applied to a wide range of systems such as polymer, covalent, metallic, and metal oxide/hydride/carbide materials[49-50].

The aim of the current work was first to develop a ReaxFF reactive force field for $BaTiO_3$, which would enable us, for example, to evaluate the influence of surface chemistry on ferroelectric response. Using this force field, we performed MD simulations to represent the phase transition sequence, ferroelectric and thermal hysteresis loops for the $BaTiO_3$ crystal structure. Furthermore, we investigated the effects of sample thickness, OVs and water medium on the domain wall and material polarization.

View Article Online
DOI: 10.1039/C9CP02955A

Methods

The ReaxFF reactive force field for $BaTiO_3$ was developed by training against a DFT derived training set including equations of state for tetragonal and cubic $BaTiO_3$ phases, OV energies and their migration barriers and asymmetric-symmetric-asymmetric $BaTiO_3$ unit cell conversion. Additionally, the *Ti* and *Ba* metal data and TiO_2 and BaO oxide data [51-52] were included in the ReaxFF training set, which extends the transferability of the developed force field to BaO and TiO_2 materials. We mainly focused on training our force field against the tetragonal and cubic phases since most of the electronic devices work in these phases. Figure 1 compares the ReaxFF and DFT results for volume/energy equations of state for ferroelectric and non-ferroelectric $BaTiO_3$ phases indicating that ReaxFF values are in very good agreement with the calculated DFT values. DFT calculations were performed using the SEQQUEST code with the generalized gradient functional as formulated by Perdew, Burke and Ernzerhof (PBE and $6 \times 6 \times 6$ *k*-point grid. Note that the current ReaxFF formulation was focused on the tetragonal and cubic phases, therefore, it cannot correctly predict the orthorhombic and rhombohedral phases to be lower in energy than the tetragonal phases.

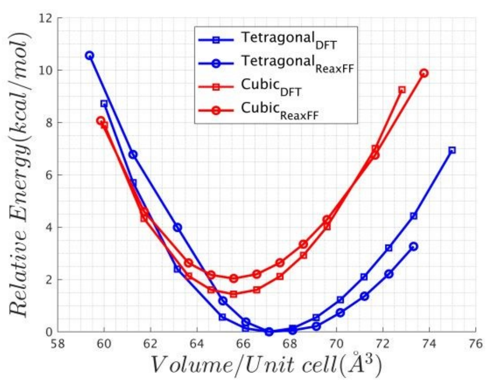

Figure 1. Comparison of DFT/PBE and ReaxFF equations of state for ferroelectric and non-ferroelectric $BaTiO_3$ crystal morphologies.

Also, ReaxFF estimates a +146.5 *kcal/mol* vacancy energy relative to O_2 for $BaTiO_3$, that is in good agreement with the corresponding DFT value of +182.6 *kcal/mol* considering that DFT

View Article Online
DOI: 10.1039/C9CP02955A

usually over-estimates the O_2 stability. Figure 2.a illustrates the lowest energy path for OV migration in $BaTiO_3$. As shown in Figure 2.a, ReaxFF predicts the energy barrier for OV migration very well (ReaxFF: 19.6 *kcal/mol*; DFT: 19.9 *kcal/mol*) which shows that ReaxFF should be capable of describing the OV migration and re-organization. The DFT calculations were performed using Vienna Ab initio Simulation Package (VASP) with the generalized gradient approximation (GGA) according to Perdew, Burke, and Ernzerhof revised for solids (PBESol) and the projector augmented-wave method. Oxygen-vacancy formation energy calculations employed a 40-atom $2 \times 2 \times 2$ as well as a 135-atom $3 \times 3 \times 3$ supercell of $BaTiO_3$. The fully relaxed static transition energy barrier for a neutral oxygen vacancy was obtained employing the nudged elastic band method (NEB) where the residue NEB forces on the atoms were less than 0.05 eV/Å in a $2 \times 2 \times 2$ supercell. A converged Γ point centered **k**-point mesh corresponding to 1.7 (1/Å) per atom was used for Brillouin zone integration and a plane wave energy cut off of 400 eV was used in all calculations. The structural relaxations were performed until the residual force of each atom was less than 0.01 eV/Å. Moreover, we could force a $BaTiO_3$ unit cell to transform from a tetragonal to a cubic structure using local restraints and based on DFT calculations, the barrier for this asymmetric to symmetric distortion is 2.1 *kcal/mol*; ReaxFF predicts a 2.0 *kcal/mol* barrier where the cubic state has the highest energy along the conversion path (Figure 2.b). The later DFT calculations were completed using the VASP with PBEsol functional, $6 \times 6 \times 6$ *k*-point mesh, 600 eV plane-wave cutoff, and 1×10^{-6} eV energy error threshold.

View Article Online
DOI: 10.1039/C9CP02955A

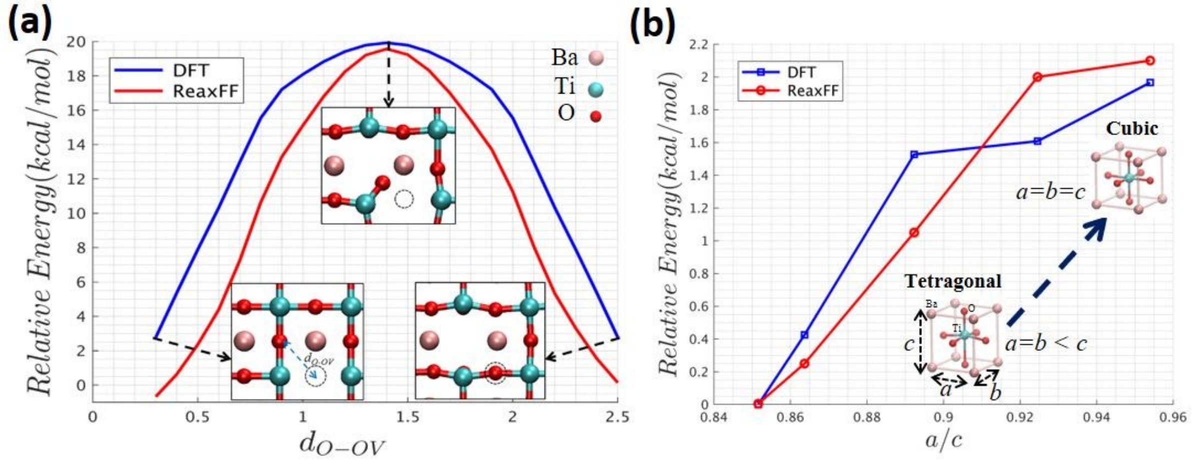

Figure 2. a): Comparison of DFT and ReaxFF energy barrier for OV migration. b): Comparison of DFT and ReaxFF energy for BaTiO3 tetragonal to cubic phase conversion.

To derive the phase diagram and the thermal hysteresis loop of the $BaTiO_3$ crystal structure, *NPT-MD* simulations were carried out on a 6 × 6 × 6 periodic $BaTiO_3$ supercell (Figure 3.a). For this purpose, the system was heated up, and subsequently cooled down both for 250 *ps* using a time step of 0.25 *fs* using a linear temperature regime in which $dT/dt = 0.002$ *K/fs* and the temperature was controlled by Berendsen thermostats and barostats with relatively weak coupling (100 *fs* for the thermostat, 2500 *fs* for the barostat coupling). The local polarization of each unit-cell $P_u(t)$ was defined as:

$$P_u(t) = \frac{1}{V_u}\left(Z^*_{Ti} r_{Ti}(t) + \frac{1}{8} Z^*_{Ba} \sum_{i=1}^{8} r_{Ba,i}(t) + \frac{1}{2} Z^*_{O} \sum_{i=1}^{6} r_{O,i}(t) \right)$$

where V_u is the volume of the unit cell Z^*_{Ti}, Z^*_{Ba} and Z^*_O are the charges of the *Ti*, *Ba* and *O* atoms obtained using the Electron Equilibration Method (EEM) approach in ReaxFF, and $r_{Ti,i}(t)$, $r_{Ba,i}(t)$ *and* $r_{O,i}(t)$ are the positions of the *Ti*, *Ba* and *O* atoms of each unit cell at time *t*.

Results and Discussion

Figure 3.b shows that ReaxFF can successfully reproduce the tetragonal and cubic phases with a phase transition temperature at T_c=240 *K*. Figure 3.c shows the total polarization of the system

View Article Online
DOI: 10.1039/C9CP02955A

for the heat up/cool down cycle, in which the hysteresis of the phase transition confirms the first-order nature of the cubic-to- tetragonal phase transition. As Figure 3.d shows, below 240 *K*, the polarization of each unit cell is along the [010] direction (*Px = Pz=0, Py >0*) which is characteristic of the tetragonal phase. Our potential only considers the tetragonal and cubic phases, however, this does not affect the practical application of the ReaxFF potential since these are the phases that are relevant for most of the applications of this materials and these phases are the main ones related to the working conditions of electronic devices.

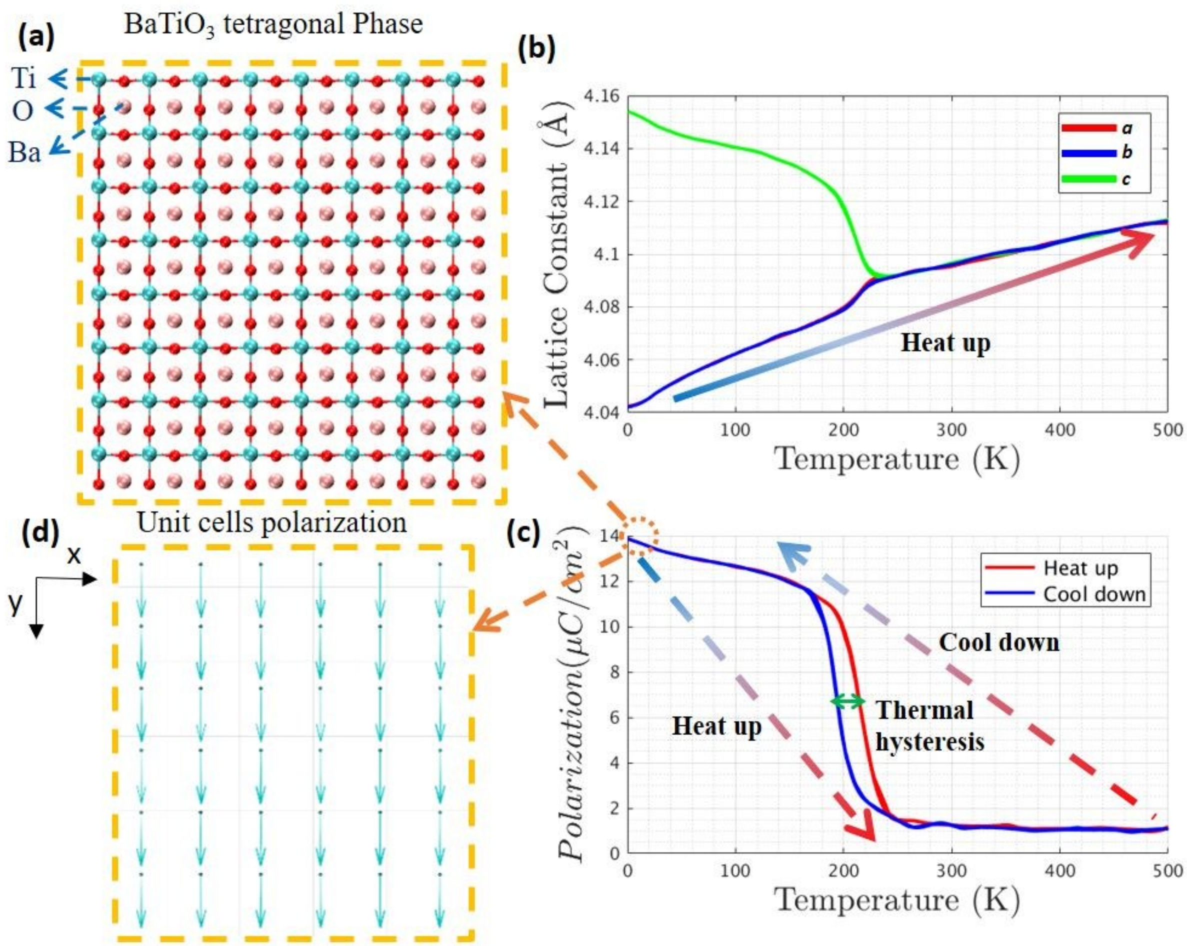

Figure 3. a) The 6 × 6 × 6 periodic $BaTiO_3$ supercell. b) Temperature dependence of the lattice constants with the phase transition from tetragonal to cubic at 240K. c) Total polarization vs temperature showing the first-order nature of the cubic-to- tetragonal phase transition. d) demonstration of unit cell polarizations in tetragonal phase in which they are all aligned in one direction.

View Article Online
DOI: 10.1039/C9CP02955A

The ferroelectric/non-ferroelectric phase transition temperature predicted by ReaxFF is closer to the experimental value compared to the calculated values by other potentials such as the shell and bond valence model listed in Table 1. The ferroelectric/non-ferroelectric phase transition temperature predicted by all potentials listed in Table 1 are underestimated since the precision of DFT methods depends on the exchange-correlation functionals and almost all DFT calculations underestimate the energy barriers between states of different phases[40, 53-54]. Moreover, we observe that ReaxFF generally predicts a lower energy than DFT along the tetragonal to cubic phase conversion path (Figure 2.b), which could explain why a lower phase transition temperature is predicted by ReaxFF compared to the reference values reported in Table 1. Also, the lattice constants and spontaneous polarization predicted by ReaxFF are in good agreement with the values obtained by experimental and numerical/theoretical methods (Table 1).

Table 1. Comparison of lattice constants and unit cell polarization of $BaTiO_3$ tetragonal and cubic phases predicted by ReaxFF with DFT, experiment and other potentials.

Parameter		**Shell**[23]	**BV**[40]	**ReaxFF**	**Experiment**	**DFT**	
Lattice constants (*A*)	**Tetragonal**					Literature	Our work
	a=b	4.002	4.005	4. 041	3.999[55]	3.966[56], 3.943[57], 3.985[40]	4.024
	c	4.043	4.109	4.155	4.036[55]	4.035[56], 3.994[57], 4.089[40]	4.206
	Cubic						
	a	4.016	4.037	4.091	4.012[58], 4.000[59]	4.002[40]	4.033
P_s ($\mu C/cm^2$)		17	28	14	26[60], 27[61], 17[55]	22.9[57], 29[56]	
T_c (K)		160	160	240	393[53]		

Due to the rapid and continuous demand for miniaturization of electronic devices, the technology of ferroelectrics moved toward thin nanometer scale films[1, 62-63]. However, the reduction of the ferroelectric size to the nanoscale significantly affects the polarization which limits the

View Article Online
DOI: 10.1039/C9CP02955A

miniaturization process[62-63]. Investigations on the physics of ultrathin ferroelectric films and specially the critical size for ferroelectricity have attracted significant attention[35-36, 62-65]. It was thought for a long time that ferroelectricity was suppressed in ultrathin films, and samples below a critical size of few tens of nanometers could not sustain a spontaneous polarization[62], however, recent experimental and numerical studies could identify ferroelectricity in much thinner films than previously thought[63, 66-67]. In our study, we used our developed force field for $BaTiO_3$ to first derive the ferroelectric hysteresis loop by applying an electric field on a $BaTiO_3$ slab with [0 0 1] surfaces and then identify the minimum thickness required to observe the ferroelectricity. Figure 4 depicts the hysteresis loops obtained by applying electric field on $BaTiO_3$ slabs with different thicknesses. The hysteresis loops for films thicker than 4.8 *nm* clearly show the remnant polarization, the saturation polarization, and the reversal electric field which are characteristics of a ferroelectric material. The results reveal the thickness dependency of the polarization in $BaTiO_3$ thin films. Based on our results a minimum thickness of 4.8 *nm* is required to observe the ferroelectric hysteresis effect which is in very good agreement with the 4.4 *nm* value found by experimental investigations[67].

View Article Online
DOI: 10.1039/C9CP02955A

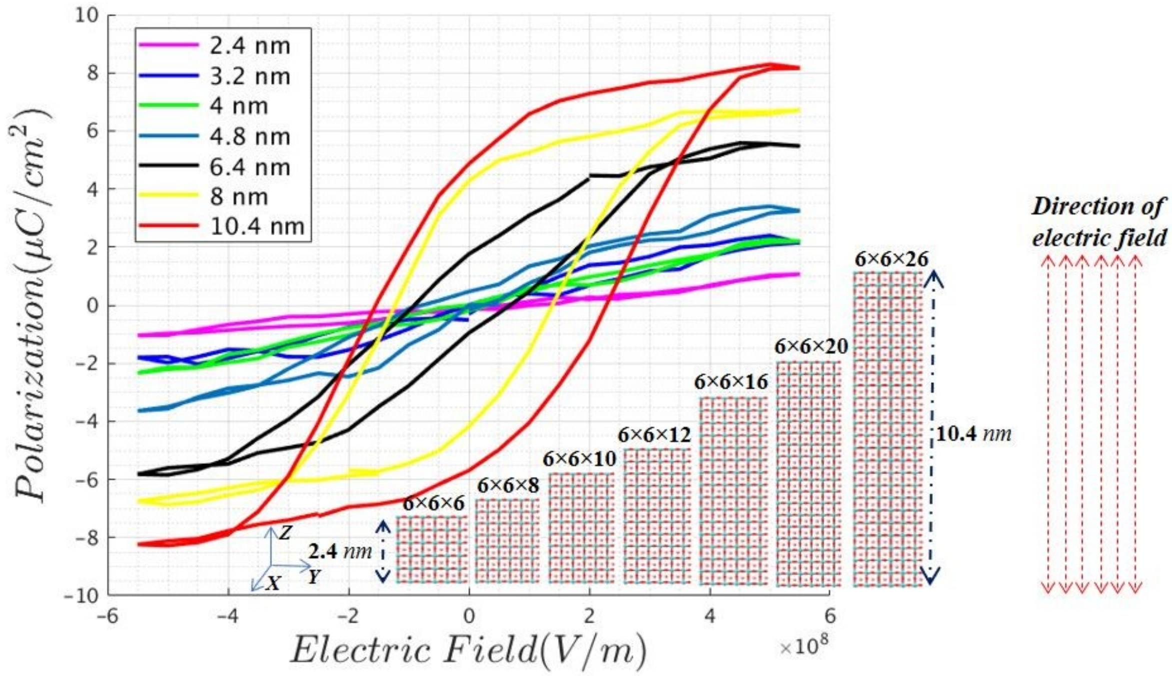

Figure 4. The hysteresis loop obtained by applying electric field on the $BaTiO_3$ slabs with different thickness. A minimum thickness of 4.8 nm is required to observe the ferroelectric hysteresis effect.

Vacancies can significantly affect the behavior and performance of ferroelectrics in capacitors, memories, and energy conversion devices[68-69]. Particularly, defects can deteriorate the polarization and cause fatigue after frequent polarization switching[68, 70]. However, defects sometimes can cause useful properties that do not exist in pure crystals [71-72]. For instance, appropriate concentration of vacancies can increase the conductivity in $SrTiO_3$ which is otherwise difficult to achieve by other methods[71, 73-74]. Also, using defect mediated reversible domain switching in aged $BaTiO_3$, large recoverable strain under low electric field can be generated[72]. The lack of an accurate and computationally inexpensive method which can reliably predict the physical properties of defective $BaTiO_3$ has hampered further progress, especially for large length and time scales phenomena. In this study, we used our developed force field to find how the OVs in $BaTiO_3$ interact with each other by running *NPT-MD* simulation at 1000K on a 6 × 6 × 6 periodic $BaTiO_3$ supercell including 5 OVs. As Figure 5.a shows, the OVs were initially

View Article Online
DOI: 10.1039/C9CP02955A

at least 12 (A) away from each other, however, after running the simulation for 2.25 *ns*, the OVs attracted each other and tend to form a cluster (Figure 5.b). Previous studies also reported that OVs in barium strontium cobalt iron oxide (BSCF) tend to form cluster arrangements[75].

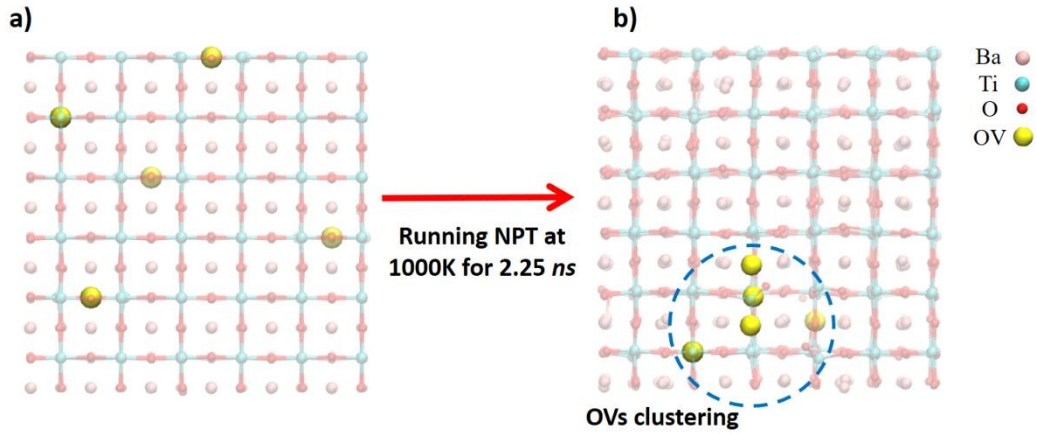

Figure 5. (a) OVs were designed to be at least 12 (A) far from each other. (b) clustering of OVs after running NPT-MD simulation at 1000K for 2.25 ns.

Also, we evaluated the vacancy formation energetics in cubic $BaTiO_3$ as a further verification of the $BaTiO_3$ ReaxFF force field. We calculated the formation energies of the oxygen, barium and titanium vacancies using the following equation:

$$E_f^d = E^{defected} - E^{pristine} - \sum_{i\,=\,Ba,\,Ti,\,O} \mu_i N_i$$

where $E^{defected}$ and $E^{pristine}$ are the total energy of the defective and reference systems, respectively, and N_i terms shows the difference in the number of *Ba, Ti* and *O* atoms in the defected and pristine structures and μ_i terms represent the chemical potentials of *Ba*, *Ti* and *O* atoms referenced to *Ba bcc* lattice, *Ti hcp* lattice and the O_2 dimer, respectively. Table 2 compares the calculated defect formation energies of *Ba*, *Ti* and *O* defects within ReaxFF and the DFT values reported by Erhart et al[76]., showing very good agreement. Also, as listed on Table 2 the calculated chemical potentials by ReaxFF for *Ba*, *Ti* and O atoms are -1.73, -4.98, -2.8 *eV/atom*, in close agreement with the experimental values of -1.87 *eV/atom* for *Ba*, -4.85

View Article Online
DOI: 10.1039/C9CP02955A

eV/atom for *Ti* and -2.58 *eV/atom* for O[76]. Based on the results, the oxygen vacancy (OV) is the most energetically favorable defect which can happen even at room temperature.

Table 2. Defect formation energies and chemical potentials predicted by ReaxFF compared with DFT and experimental values.

	$Formation\ Energy\ (eV/mol)$				$Chemical\ Potential\ (eV/atom)$		
	E_f^O	E_f^{Ba}	E_f^{Ti}		μ_{Ba}	μ_{Ti}	μ_O
$ReaxFF$	9.07	9.80	17.94	$ReaxFF$	-1.73	-4.98	-2.8
DFT[76]	8.22	10.25	14.55	$Experiment$[76]	-1.87	-4.85	-2.58

Moreover, we used our developed force field to investigate the effects of different concentration of OVs on the initial polarization and the phase transition temperature. Table 3 shows the effects of the OVs on the initial polarization (P_i) and the phase transition temperature (T_c). Based on our findings, by increasing the OV concentration in the system, the phase transition temperature and the initial polarization decrease monotonically. For instance, 0.5 % and 1.0 % OV in the system decrease the initial polarization from the initial value of 14 $\mu C/cm^2$ to 12.95 $\mu C/cm^2$ and 11.52 $\mu C/cm^2$, respectively, and the phase transition temperature from 240 *K* to 180 *K* and 150 *K*. Other MD and *ab-initio* studies also observed that OVs decrease the phase transition temperature and the initial polarization of the $BaTiO_3$ structure [27, 32, 77]. OV induced polarization loss in ferroelectrics is because OVs distort the polarization of the unit cells, therefore, the polarization of such unit cells can be hardly rectified in the original direction[32]. Moreover, the polarization can be pinned to a specific direction by OVs which leads to tail-to-tail polarizations along the *Ti-OV-Ti* pattern and suppression of the total polarization[77].

Table 3. The effect of the OVs on the initial polarization and the phase transition temperature.

% OV	***P_i ($\mu C/cm^2$)***	***T_c (K)***
0	14	240
0.5	12.95	180
1	11.52	150
1.5	10.54	140
2	7.80	130

View Article Online
DOI: 10.1039/C9CP02955A

Ferroelectrics are composed of domains of different polarization orientations, separated by domain walls. The normal component of spontaneous polarization is usually continuous across the domain walls to minimize the polarization charges ($-\nabla \cdot P$) and meet the electrostatic compatibility condition[78]. These are called neutral domain walls (NDW) as they exhibit no net bound charges. On the other hand, charged domain walls (CDW) exhibit net polarization bound charges due to the discontinuity of polarizations across the domain walls [78]. Figure 6.a shows the capability of ReaxFF to predict a head-to-head 180° charged domain wall formation in a 14.4 *nm* thick $BaTiO_3$ slab with TiO_2 [0 0 1] surfaces. Due to TiO_2 [0 0 1] surfaces, negative unscreened bound charges exist on the surfaces of the $BaTiO_3$ slab creating a charged domain wall in the middle of the slab which violates the condition of electrostatic compatibility [78]. This observation indicates that our force field can be utilized to study the complex dynamics of domain walls in $BaTiO_3$.

Uniquely, ReaxFF allows us to evaluate the effects of surface chemistry on domain wall structure and mobility. Water molecules are easily adsorbed on $BaTiO_3$ surfaces and change their physical properties. Therefore, the atomistic scale study of the water adsorption on ferroelectric surfaces is crucial for the advance in the understanding of $BaTiO_3$ ferroelectrics properties and can benefit the associated applications[79-80]. Previous investigations indicated that the charge screening induced by molecular adsorbates such as hydroxyl, carboxylate and oleic acid can stabilize the ferroelectricity and decrease the critical size in $BaTiO_3$ nanowires and nanoparticles[20, 81]. We utilized our developed force field to investigate the effects of a water medium on the polarization of a 14.4 *nm* thick $BaTiO_3$ slab with TiO_2 [0 0 1] surfaces, by adding water molecules around surfaces and running MD simulations for 0.5 *ns*. As Figure 6.b shows, the water molecules are adsorbed on the surfaces and dissociated into hydroxyl groups.

View Article Online
DOI: 10.1039/C9CP02955A

Therefore, surfaces are screened by the adsorption of water molecules on the surfaces causing the polarization rearrangement in the $BaTiO_3$ slab[82]. As Figure 6 shows, adding water molecules leads to an increased amount of polarization from 4.6 $\mu C/cm^2$ to 12.5 $\mu C/cm^2$ due to the charge screening induced by adsorption of water molecules on the surfaces of $BaTiO_3$ slab[82]. Additionally, as Figure 6.b shows, dissociative adsorption of water molecules on the surfaces leads to a 90° domain switching compared to Figure 6.a in which domains are aligned in the z direction. Such an observation was reported by Li et al. in which using *ab-initio* method they showed that when the water molecules are dissociatively adsorbed on the TiO_2 terminated surfaces, a 90° surface domain switching occurs[82]. Our results indicate that our developed force field can be successfully used to study the interactions of $BaTiO_3$ in multi-material interfaces and its related applications.

View Article Online
DOI: 10.1039/C9CP02955A

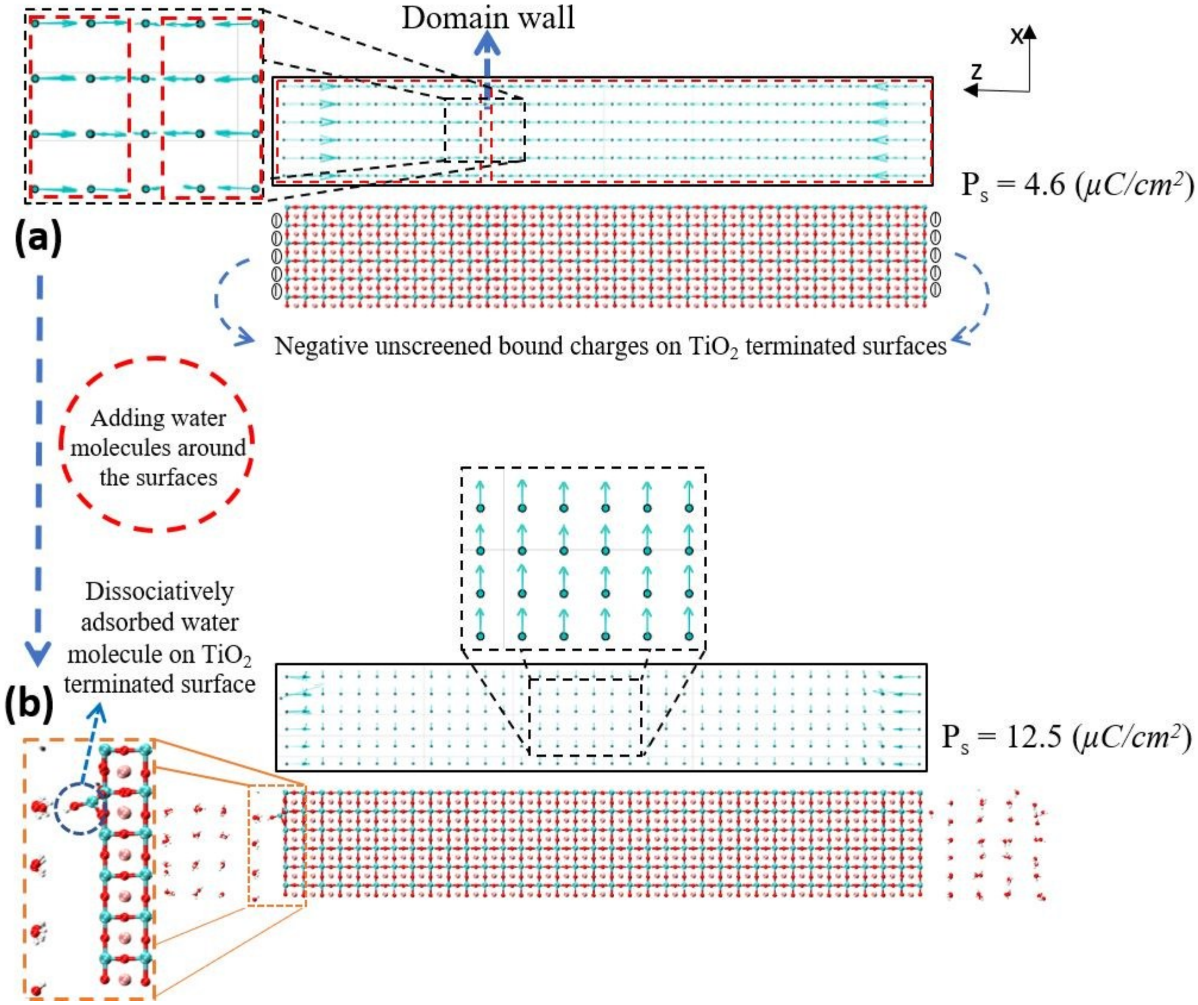

Figure 6. (a) Demonstration of a head-to-head 180° charged domain wall formation in a 14.4 *nm* thick $BaTiO_3$ slab with TiO_2 [0 0 1] surfaces. Due to TiO_2 [0 0 1] surfaces, negative unscreened bound charges exist on the surfaces of the $BaTiO_3$ slab creating a charged domain wall near the middle of the slab. (b) Adding water molecules around the surfaces leads to an increased amount of polarization from 4.6 $\mu C/cm^2$ to 12.5 $\mu C/cm^2$ due to the charge screening induced by adsorption of water molecules on the surfaces. Moreover, this leads to a 90° domain switching compared to the surface condition in Figure 6.a in which domains are aligned in the z direction.

Conclusion

As a conclusion, we successfully developed the ReaxFF description to the ferroelectric and non-ferroelectric phases for $BaTiO_3$. This extension was performed without any modification in the ReaxFF functional form which means that this $BaTiO_3$ parameter set can be straightforwardly extended to a wide range of other ferroelectric oxides, including those with crystal phase stabilities that are highly sensitive to defects and strain, such as orthorhombic HfO_2/ZrO_2, providing a unique and computationally inexpensive simulation tool for realistic ferroelectric

View Article Online
DOI: 10.1039/C9CP02955A

materials. OVs and their migration were also considered in the force field development. Given that realistic $BaTiO_3$ materials have a significant concentrations of defects, this again extends the realism of the ReaxFF description. We tested the ReaxFF $BaTiO_3$ parameter set in a series of MD simulation, which reproduced a reversible ferroelectric/non-ferroelectric phase transition upon heating and cooling. Using our developed force field, we found a minimum thickness of 4.8 *nm* is required to observe the ferroelectric hysteresis effect. Also, we indicated that OVs in $BaTiO_3$ tend to form a cluster and reduce the polarization and the phase transition temperature. Moreover, the $BaTiO_3$ ReaxFF reactive force field has the capability of predicting the dynamics of neutral and charged domain walls in $BaTiO_3$. Finally, we found that charge screening induced by adsorption of water molecules on the TiO_2 terminated surfaces of a $BaTiO_3$ slab leads to a 90° domain switching and an increased amount of polarization comparing to a $BaTiO_3$ slab with unscreened TiO_2 terminated surfaces. The satisfactory comparison of the ReaxFF results with available experimental and *ab-initio* data indicates the robustness and capabilities of the new ReaxFF reactive potential. Our encouraging results should allow us to further investigate the role of such point-defects on domain-motion, switching and piezoelectric and other linear as well as non-linear field-responses using the ReaxFF force-field formalism, and this can be tremendously useful for a wide range of technological applications involving ferroelectric interfaces in energy-conversion, electronic and neuromorphic systems.

Acknowledgements We acknowledge funding from AFRL grant FA9451-16-1-0041. PG was supported by the Center for Nanophase Materials Sciences (CNMS), which is a US DOE Office of Science User Facility, located at Oak Ridge National Laboratory. J.M.M. and I.D. acknowledge support from the Natural Sciences and Engineering Research Council of Canada (NSERC) and the National Science Foundation under Grant No. 1807768, respectively.

View Article Online
DOI: 10.1039/C9CP02955A

References

1. Rabe, K. M.; Ahn, C. H.; Triscone, J.-M., *Physics of ferroelectrics: a modern perspective*. Springer Science & Business Media: 2007; Vol. 105.
2. Xu, Y., *Ferroelectric materials and their applications*. Elsevier: 2013.
3. Cross, L. E., Ferroelectric materials for electromechanical transducer applications. *Materials chemistry and physics* **1996,** *43* (2), 108-115.
4. Bowen, C.; Kim, H.; Weaver, P.; Dunn, S., Piezoelectric and ferroelectric materials and structures for energy harvesting applications. *Energy & Environmental Science* **2014,** *7* (1), 25-44.
5. Setter, N.; Damjanovic, D.; Eng, L.; Fox, G.; Gevorgian, S.; Hong, S.; Kingon, A.; Kohlstedt, H.; Park, N.; Stephenson, G., Ferroelectric thin films: Review of materials, properties, and applications. *Journal of Applied Physics* **2006,** *100* (5), 051606.
6. Zhang, Y.; Lu, H.; Xie, L.; Yan, X.; Paudel, T. R.; Kim, J.; Cheng, X.; Wang, H.; Heikes, C.; Li, L., Anisotropic polarization-induced conductance at a ferroelectric–insulator interface. *Nature nanotechnology* **2018,** *13* (12), 1132.
7. Chanthbouala, A.; Garcia, V.; Cherifi, R. O.; Bouzehouane, K.; Fusil, S.; Moya, X.; Xavier, S.; Yamada, H.; Deranlot, C.; Mathur, N. D., A ferroelectric memristor. *Nature materials* **2012,** *11* (10), 860.
8. Rumpf, H.; Modrow, H.; Hormes, J.; Gläsel, H.-J.; Hartmann, E.; Erdem, E.; Böttcher, R.; Hallmeier, K.-H., Preparation of nanocrystalline BaTiO3 characterized by in situ X-ray absorption spectroscopy. *The Journal of Physical Chemistry B* **2001,** *105* (17), 3415-3421.
9. Erdem, E.; Semmelhack, H.-C.; Böttcher, R.; Rumpf, H.; Banys, J.; Matthes, A.; Gläsel, H.-J.; Hirsch, D.; Hartmann, E., Study of the tetragonal-to-cubic phase transition in PbTiO3 nanopowders. *Journal of Physics: Condensed Matter* **2006,** *18* (15), 3861.
10. Erdem, E.; Jakes, P.; Parashar, S.; Kiraz, K.; Somer, M.; Rüdiger, A.; Eichel, R.-A., Defect structure in aliovalently-doped and isovalently-substituted PbTiO3 nano-powders. *Journal of Physics: Condensed Matter* **2010,** *22* (34), 345901.
11. Erdem, E.; Kiraz, K.; Somer, M.; Eichel, R.-A., Size effects in Fe3+-doped PbTiO3 nanocrystals—Formation and orientation of (FeTi′ VO) defect-dipoles. *Journal of the European Ceramic Society* **2010,** *30* (2), 289-293.
12. Bi, M.; Hao, Y.; Zhang, J.; Lei, M.; Bi, K., Particle size effect of BaTiO 3 nanofillers on the energy storage performance of polymer nanocomposites. *Nanoscale* **2017,** *9* (42), 16386-16395.
13. Suematsu, K.; Arimura, M.; Uchiyama, N.; Saita, S.; Makino, T., High-performance dielectric thin film nanocomposites of barium titanate and cyanoethyl pullulan: controlling the barium titanate nanoparticle size using a sol–gel method. *RSC Advances* **2016,** *6* (25), 20807-20813.
14. Jiang, B.; Iocozzia, J.; Zhao, L.; Zhang, H.; Harn, Y.-W.; Chen, Y.; Lin, Z., Barium titanate at the nanoscale: controlled synthesis and dielectric and ferroelectric properties. *Chemical Society Reviews* **2019,** *48* (4), 1194-1228.
15. Devonshire, A. F., XCVI. Theory of barium titanate: Part I. *The London, Edinburgh, and Dublin Philosophical Magazine and Journal of Science* **1949,** *40* (309), 1040-1063.
16. Devonshire, A. F., CIX. Theory of barium titanate—Part II. *The London, Edinburgh, and Dublin Philosophical Magazine and Journal of Science* **1951,** *42* (333), 1065-1079.
17. Chen, L. Q., Phase-field method of phase transitions/domain structures in ferroelectric thin films: a review. *Journal of the American Ceramic Society* **2008,** *91* (6), 1835-1844.
18. Cohen, R.; Krakauer, H., Lattice dynamics and origin of ferroelectricity in BaTiO 3: Linearized-augmented-plane-wave total-energy calculations. *Physical Review B* **1990,** *42* (10), 6416.
19. Piskunov, S.; Heifets, E.; Eglitis, R.; Borstel, G., Bulk properties and electronic structure of SrTiO3, BaTiO3, PbTiO3 perovskites: an ab initio HF/DFT study. *Computational Materials Science* **2004,** *29* (2), 165-178.

View Article Online
DOI: 10.1039/C9CP02955A

20. Spanier, J. E.; Kolpak, A. M.; Urban, J. J.; Grinberg, I.; Ouyang, L.; Yun, W. S.; Rappe, A. M.; Park, H., Ferroelectric phase transition in individual single-crystalline BaTiO3 nanowires. *Nano letters* **2006,** *6* (4), 735-739.
21. Kolpak, A. M.; Li, D.; Shao, R.; Rappe, A. M.; Bonnell, D. A., Evolution of the structure and thermodynamic stability of the BaTiO 3 (001) surface. *Physical review letters* **2008,** *101* (3), 036102.
22. Khatib, D.; Migoni, R.; Kugel, G.; Godefroy, L., Lattice dynamics of BaTiO3 in the cubic phase. *Journal of Physics: Condensed Matter* **1989,** *1* (49), 9811.
23. Tinte, S.; Stachiotti, M.; Sepliarsky, M.; Migoni, R.; Rodriguez, C., Atomistic modelling of BaTiO3 based on first-principles calculations. *Journal of Physics: Condensed Matter* **1999,** *11* (48), 9679.
24. Tinte, S.; Stachiotti, M.; Sepliarsky, M.; Migoni, R.; Rodriguez, C., Order-disorder, local structure and precursor effects in BaTiO3. *Ferroelectrics* **2000,** *237* (1), 41-48.
25. Tinte, S.; Stachiotti, M. G., Surface effects and ferroelectric phase transitions inBaTiO3ultrathin films. *Physical Review B* **2001,** *64* (23).
26. Sepliarsky, M.; Tinte, S., Dynamical behavior of the phase transition of strained from atomistic simulations. *Physica B: Condensed Matter* **2009,** *404* (18), 2730-2732.
27. Chen, Y.; Liu, B.; Ma, Y.; Zhou, Y., Modification of a shell model for the study of the radiation effects in BaTiO3. *Nuclear Instruments and Methods in Physics Research Section B: Beam Interactions with Materials and Atoms* **2009,** *267* (18), 3090-3093.
28. Gonçalves, L. G. V.; Rino, J. P., Finite size effects on a core-shell model of barium titanate. *Computational Materials Science* **2017,** *130*, 98-102.
29. Zhang, Y.; Hong, J.; Liu, B.; Fang, D., Strain effect on ferroelectric behaviors of BaTiO3 nanowires: a molecular dynamics study. *Nanotechnology* **2010,** *21* (1), 015701.
30. Zhang, Y.; Hong, J.; Liu, B.; Fang, D., Molecular dynamics investigations on the size-dependent ferroelectric behavior of BaTiO3 nanowires. *Nanotechnology* **2009,** *20* (40), 405703.
31. Sang, Y.; Liu, B.; Fang, D., The size and strain effects on the electric-field-induced domain evolution and hysteresis loop in ferroelectric BaTiO3 nanofilms. *Computational Materials Science* **2008,** *44* (2), 404-410.
32. Wang, J.; Shen, Y.; Song, F.; Ke, F.; Bai, Y.; Lu, C., Effects of oxygen vacancies on polarization stability of barium titanate. *Science China Physics, Mechanics & Astronomy* **2016,** *59* (3).
33. Zhong, W.; Vanderbilt, D.; Rabe, K. M., Phase transitions in BaTiO3 from first principles. *Phys Rev Lett* **1994,** *73* (13), 1861-1864.
34. Zhong, W.; Vanderbilt, D.; Rabe, K., First-principles theory of ferroelectric phase transitions for perovskites: The case of BaTiO 3. *Physical Review B* **1995,** *52* (9), 6301.
35. Paul, J.; Nishimatsu, T.; Kawazoe, Y.; Waghmare, U. V., Ferroelectric phase transitions in ultrathin films of BaTiO3. *Phys Rev Lett* **2007,** *99* (7), 077601.
36. Nishimatsu, T.; Waghmare, U. V.; Kawazoe, Y.; Vanderbilt, D., Fast molecular-dynamics simulation for ferroelectric thin-film capacitors using a first-principles effective Hamiltonian. *Physical Review B* **2008,** *78* (10), 104104.
37. Paul, J.; Nishimatsu, T.; Kawazoe, Y.; Waghmare, U., A first-principles study of phase transitions in ultrathin films of BaTiO 3. *Pramana* **2008,** *70* (2), 263-270.
38. Paul, J.; Nishimatsu, T.; Kawazoe, Y.; Waghmare, U. V., Polarization switching in epitaxial films of BaTiO3: A molecular dynamics study. *Applied Physics Letters* **2008,** *93* (24), 242905.
39. Grünebohm, A.; Nishimatsu, T., Influence of defects on ferroelectric and electrocaloric properties of BaTiO 3. *Physical Review B* **2016,** *93* (13), 134101.
40. Qi, Y.; Liu, S.; Grinberg, I.; Rappe, A. M., Atomistic description for temperature-driven phase transitions in BaTiO 3. *Physical Review B* **2016,** *94* (13), 134308.

View Article Online
DOI: 10.1039/C9CP02955A

41. Liu, S.; Grinberg, I.; Rappe, A. M., Development of a bond-valence based interatomic potential for BiFeO3 for accurate molecular dynamics simulations. *Journal of Physics: Condensed Matter* **2013,** *25* (10), 102202.
42. Shin, Y.-H.; Cooper, V. R.; Grinberg, I.; Rappe, A. M., Development of a bond-valence molecular-dynamics model for complex oxides. *Physical Review B* **2005,** *71* (5), 054104.
43. Shin, Y.-H.; Son, J.-Y.; Lee, B.-J.; Grinberg, I.; Rappe, A. M., Order–disorder character of PbTiO3. *Journal of Physics: Condensed Matter* **2007,** *20* (1), 015224.
44. Liu, S.; Grinberg, I.; Takenaka, H.; Rappe, A. M., Reinterpretation of the bond-valence model with bond-order formalism: An improved bond-valence-based interatomic potential for PbTiO 3. *Physical Review B* **2013,** *88* (10), 104102.
45. Goddard III, W. A.; Zhang, Q.; Uludogan, M.; Strachan, A.; Cagin, T. In *The ReaxFF polarizable reactive force fields for molecular dynamics simulation of ferroelectrics*, AIP Conference Proceedings, AIP: 2002; pp 45-55.
46. Van Duin, A. C.; Dasgupta, S.; Lorant, F.; Goddard, W. A., ReaxFF: a reactive force field for hydrocarbons. *The Journal of Physical Chemistry A* **2001,** *105* (41), 9396-9409.
47. Chenoweth, K.; Van Duin, A. C.; Goddard, W. A., ReaxFF reactive force field for molecular dynamics simulations of hydrocarbon oxidation. *The Journal of Physical Chemistry A* **2008,** *112* (5), 1040-1053.
48. Mortier, W. J.; Ghosh, S. K.; Shankar, S., Electronegativity-equalization method for the calculation of atomic charges in molecules. *Journal of the American Chemical Society* **1986,** *108* (15), 4315-4320.
49. Senftle, T. P.; Hong, S.; Islam, M. M.; Kylasa, S. B.; Zheng, Y.; Shin, Y. K.; Junkermeier, C.; Engel-Herbert, R.; Janik, M. J.; Aktulga, H. M., The ReaxFF reactive force-field: development, applications and future directions. *npj Computational Materials* **2016,** *2*, 15011.
50. Kowalik, M.; Ashraf, C.; Damirchi, B.; Akbarian, D.; Rajabpour, S.; van Duin, A. C. T., Atomistic Scale Analysis of the Carbonization Process for C/H/O/N-Based Polymers with the ReaxFF Reactive Force Field. *The Journal of Physical Chemistry B* **2019,** *123* (25), 5357-5367.
51. van Duin, A. C. T.; Merinov, B. V.; Han, S. S.; Dorso, C. O.; Goddard, W. A., ReaxFF Reactive Force Field for the Y-Doped BaZrO3 Proton Conductor with Applications to Diffusion Rates for Multigranular Systems. *Journal of Physical Chemistry A* **2008,** *112* (45), 11414-11422.
52. Kim, S.-Y.; Kumar, N.; Persson, P.; Sofo, J.; van Duin, A. C. T.; Kubicki, J. D., Development of a ReaxFF reactive force field for Titanium dioxide/water systems. *Langmuir* **2013,** *29*, 7838-7846.
53. Vielma, J. M.; Schneider, G., Shell model of BaTiO3 derived from ab-initio total energy calculations. *Journal of Applied Physics* **2013,** *114* (17), 174108.
54. Liu, S.; Grinberg, I.; Rappe, A. M., Development of a bond-valence based interatomic potential for BiFeO3 for accurate molecular dynamics simulations. *J Phys Condens Matter* **2013,** *25* (10), 102202.
55. Kwei, G.; Lawson, A.; Billinge, S.; Cheong, S., Structures of the ferroelectric phases of barium titanate. *The Journal of Physical Chemistry* **1993,** *97* (10), 2368-2377.
56. Wang, J. J.; Meng, F. Y.; Ma, X. Q.; Xu, M. X.; Chen, L. Q., Lattice, elastic, polarization, and electrostrictive properties of BaTiO3 from first-principles. *Journal of Applied Physics* **2010,** *108* (3), 034107.
57. Fechner, M.; Ostanin, S.; Mertig, I., Effect of the surface polarization in polar perovskites studied from first principles. *Physical Review B* **2008,** *77* (9), 094112.
58. Kay, H. F.; Vousden, P., XCV. Symmetry changes in barium titanate at low temperatures and their relation to its ferroelectric properties. *The London, Edinburgh, and Dublin Philosophical Magazine and Journal of Science* **1949,** *40* (309), 1019-1040.
59. Hellwege, K.; Hellwege, A., Ferroelectrics and related substances, Landolt-Börnstein, New Series. *Group III* **1969,** *3*.

View Article Online
DOI: 10.1039/C9CP02955A

60. Wieder, H., Electrical behavior of barium titanatge single crystals at low temperatures. *Physical Review* **1955,** *99* (4), 1161.
61. Shirane, G.; Takeda, A., Transition energy and volume change at three transitions in barium titanate. *Journal of the Physical Society of Japan* **1952,** *7* (1), 1-4.
62. Zhao, Z.; Buscaglia, V.; Viviani, M.; Buscaglia, M. T.; Mitoseriu, L.; Testino, A.; Nygren, M.; Johnsson, M.; Nanni, P., Grain-size effects on the ferroelectric behavior of dense nanocrystalline BaTiO 3 ceramics. *Physical Review B* **2004,** *70* (2), 024107.
63. Junquera, J.; Ghosez, P., Critical thickness for ferroelectricity in perovskite ultrathin films. *Nature* **2003,** *422* (6931), 506.
64. Tenne, D. A.; Turner, P.; Schmidt, J.; Biegalski, M.; Li, Y.; Chen, L.; Soukiassian, A.; Trolier-McKinstry, S.; Schlom, D.; Xi, X., Ferroelectricity in ultrathin BaTiO 3 films: probing the size effect by ultraviolet Raman spectroscopy. *Physical review letters* **2009,** *103* (17), 177601.
65. Li, K. T.; Lo, V. C., Simulation of thickness dependence in ferroelectric thin films. *Solid state communications* **2004,** *132* (1), 49-54.
66. Wang, X.; Deng, X.; Wen, H.; Li, L., Phase transition and high dielectric constant of bulk dense nanograin barium titanate ceramics. *Applied physics letters* **2006,** *89* (16), 162902.
67. Li, Y.; Yu, R.; Zhou, H.; Cheng, Z.; Wang, X.; Li, L.; Zhu, J., Direct observation of thickness dependence of ferroelectricity in freestanding batio3 thin film. *Journal of the American Ceramic Society* **2015,** *98* (9), 2710-2712.
68. Cockayne, E.; Burton, B. P., Dipole moment of a Pb-O vacancy pair in PbTiO 3. *Physical Review B* **2004,** *69* (14), 144116.
69. Tselev, A.; Ganesh, P.; Qiao, L.; Siemons, W.; Gai, Z.; Biegalski, M. D.; Baddorf, A. P.; Kalinin, S. V., Oxygen control of atomic structure and physical properties of SrRuO3 surfaces. *ACS nano* **2013,** *7* (5), 4403-4413.
70. Zhang, Y.; Li, J.; Fang, D., Oxygen-vacancy-induced memory effect and large recoverable strain in a barium titanate single crystal. *Physical Review B* **2010,** *82* (6), 064103.
71. Tufte, O.; Chapman, P., Electron mobility in semiconducting strontium titanate. *Physical Review* **1967,** *155* (3), 796.
72. Ren, X., Large electric-field-induced strain in ferroelectric crystals by point-defect-mediated reversible domain switching. *Nature materials* **2004,** *3* (2), 91.
73. Lopez-Bezanilla, A.; Ganesh, P.; Littlewood, P. B., Magnetism and metal-insulator transition in oxygen-deficient SrTiO 3. *Physical Review B* **2015,** *92* (11), 115112.
74. Zhuang, H. L.; Ganesh, P.; Cooper, V. R.; Xu, H.; Kent, P., Understanding the interactions between oxygen vacancies at SrTiO 3 (001) surfaces. *Physical Review B* **2014,** *90* (6), 064106.
75. Gangopadhyay, S.; Masunov, A. E.; Inerbaev, T.; Mesit, J.; Guha, R. K.; Sleiti, A. K.; Kapat, J. S., Understanding oxygen vacancy migration and clustering in barium strontiumcobalt iron oxide. *Solid State Ionics* **2010,** *181* (23-24), 1067-1073.
76. Erhart, P.; Albe, K., Thermodynamics of mono-and di-vacancies in barium titanate. *Journal of Applied Physics* **2007,** *102* (8), 084111.
77. Li, M.; Li, J.; Chen, L.-Q.; Gu, B.-L.; Duan, W., Effects of strain and oxygen vacancies on the ferroelectric and antiferrodistortive distortions in PbTiO 3/SrTiO 3 superlattice. *Physical Review B* **2015,** *92* (11), 115435.
78. Bednyakov, P. S.; Sluka, T.; Tagantsev, A. K.; Damjanovic, D.; Setter, N., Formation of charged ferroelectric domain walls with controlled periodicity. *Scientific reports* **2015,** *5*, 15819.
79. Li, X.; Wang, B.; Zhang, T.-Y.; Su, Y., Water adsorption and dissociation on BaTiO3 single-crystal surfaces. *The Journal of Physical Chemistry C* **2014,** *118* (29), 15910-15918.

View Article Online
DOI: 10.1039/C9CP02955A

80. He, D.; Qiao, L.; Khodayari, M.; Volinsky, A. A., Electric field and humidity effects on adsorbed water behavior on BaTiO3 ferroelectric domains studied by scanning probe microscopy. *Journal of Applied Physics* **2014,** *116* (8), 084105.
81. Yasui, K.; Kato, K., Influence of adsorbate-induced charge screening, depolarization factor, mobile carrier concentration, and defect-induced microstrain on the size effect of a BaTiO3 nanoparticle. *The Journal of Physical Chemistry C* **2013,** *117* (38), 19632-19644.
82. Li, X.; Bai, Y.; Wang, B.; Su, Y., Water adsorption induced in-plane domain switching on BaTiO3 surface. *Journal of Applied Physics* **2015,** *118* (9), 094104.